



1,4-Dioxane degradation by oxidation and sonication in the presence of different-sized ZVI in open-air system

Jina Shin^a, Young-Chul Lee^b, Yeonghee Ahn^c, Ji-Won Yang^{d,*}

^aChungcheong Water Supply Regional Headquarters, Korea Water Resources Corporation, 1571, je-2(i)Sunhawn-ro, Heungdeok-gu, Cheongju-si, Chungbuk 361-230, Republic of Korea

^bDepartment of Chemical and Biomolecular Engineering (BK21 program), KAIST, 335 Gwahak-ro, Yuseong-gu, Daejeon 305-701, Republic of Korea

^cDepartment of Environmental Engineering, Dong-A University, 840 Hadan-dong, Saha-gu, Busan 604-714, Republic of Korea

^dAdvanced Biomass R&D Center, KAIST, 291 Daehakno, Yuseong-gu, Daejeon 305-701, Republic of Korea
Tel. +82 42 350 3924; Fax: +82 42 350 3910; email: jiwonyang@kaist.ac.kr

Received 25 January 2012; Accepted 29 March 2012

ABSTRACT

We investigated the effect of particle size during oxidation and the sono-Fenton process in an open-air system (without air supply) containing microscale zero-valent iron (MZVI) and nano-scale zero-valent iron (nZVI) on the degradation of 1,4-dioxane (1,4-D) at neutral pH. Time-dependent concentrations of 1,4-D, H₂O₂, and ionic Fe were measured as a function of MZVI and nZVI loading during oxidation and sono-Fenton (without addition of H₂O₂). The optimal loading of MZVI and nZVI for 1,4-D degradation were determined to be 0.5 g/L during both oxidation and sono-Fenton, and 0.2 and 0.1 g/L during both oxidation and sono-Fenton, respectively. Overall, the optimal loading of MZVI in both the oxidation and sono-Fenton system showed better 1,4-D degradation efficiency compared with the optimal loading of nZVI for 6 h: approximately 60.00 and 76.65% removal efficiencies for MZVI oxidation and sono-Fenton, respectively, while approximately 47.13 and 60.98% removal efficiencies for nZVI oxidation and sono-Fenton, respectively. Consequently, the smaller size of ZVI did not enhance 1,4-D degradation efficiency during the oxidation and sono-Fenton at neutral pH.

Keywords: Zero-valent iron; Size effect; Oxidation; Sono-Fenton; 1,4-Dioxane degradation

1. Introduction

The 1,4-dioxane (1,4-D) compound is widely used as a solvent and stabilizer of halogenated compounds for industrial purposes and plastic manufacturing [1], and is found in low concentrations in surfactants and shampoos [2,3]. The 1,4-D compound is not only classified as a toxic and carcinogenic pollutant but also contaminates surface water,

groundwater, and soil due to its high water solubility (4.31×10^5 mg/L), low octanol-water partition coefficient ($K_{ow} = 10^{-0.27}$), and low vapor pressure (37 mm Hg at 25°C) (see Table 1) [2,4]. Because of a recalcitrant organic associated with the heterocyclic structure of 1,4-D, the compound presents a public health threat, due to its accumulation in the water supply. The US EPA issued a drinking water health standard for 1,4-D, and Korea also enacts a drinking water regulation limiting 1,4-D concentrations to 0.05 mg/L.

*Corresponding author.

The physical removal of 1,4-D, through such means as the use of activated carbon and air stripping, is expensive and difficult, requiring secondary treatment steps. Thus, many strategies have adopted the use of the Fenton reaction as an alternative. Conventionally, homogeneous Fenton processes use ferrous (Fe^{2+}) salt and H_2O_2 to produce a nonselective attacker, $\cdot\text{OH}$ radical, to detoxify target pollutants, but it still requires a secondary process to separate massive sludge accumulated during the neutralization step prior to being discharged from water/wastewater treatment plant [4,5]. In the presence of heterogeneous iron powder, the reaction proceeds via oxidation by injection of H_2O_2 or air sparging, in which zero-valent iron (ZVI) plays a significant role as an oxidative catalyst to produce H_2O_2 and $\cdot\text{OH}$ radicals [6–8]. These result in the breaking of cyclic compounds and an improvement in the biodegradability of the intermediate compounds [2,4,9,10]. Other researchers have disclosed a mechanism of 1,4-D degradation by treatment with UV/ H_2O_2 and subsequent decomposition by sonolysis, producing ethylene glycol diformate (EGD), glyoxal, formaldehyde, and several short-chain organic acid byproducts [11,12]. Therefore, the development of an economical method of pretreatment that can break the ring structure of 1,4-D is required as one of the primary goals of 1,4-D treatment in water/wastewater plants.

Beyond the Fenton reaction in the presence of ZVI and an H_2O_2 supply, i.e. advanced oxidation process [13,14], the oxidation of ZVI in aqueous solution in the presence of oxygen can generate oxidants and subsequently degrade contaminants because of the spontaneous generation of H_2O_2 in the presence of ZVI and O_2 [5,6,15]. The ZVI oxidation process is currently suggested to be a potential process for the treatment of refractory organic pollutants. Therefore, to enhance the contaminant degradation efficiency of the ZVI oxidation system, many efforts using additives, such as ligands [16,17] and ultrasound [18–24], which is expected to increase the active surface area [25–31], have been made to reduce the iron oxide layer covering Fe^0 because fast oxidation from Fe^0 to iron oxides ($\text{Fe}_2\text{O}_3/\text{Fe}_3\text{O}_4$) decreases the degradation efficiency of target materials.

Based on those techniques, several studies using sonication to degrade various contaminants in the presence of ZVI at a neutral pH have received widespread attention. Of particular interest are those processes that include microscale zero-valent iron (MZVI) [14,18,19,22–24] and nanoscale zero-valent iron (nZVI) [29–32], which feature combinations of sonochemistry with the Fenton reaction, i.e. sono-Fenton, that accelerate the generation of H_2O_2 , depending on cavitation

and the oxidants produced by the Fenton reaction compared to conventional ZVI oxidation processes.

Recently, a few related studies regarding the Fenton reaction, oxidation with air sparging, and sono-Fenton have featured a cost evaluation [33–35]. However, a comprehensive study on the effect of ZVI size during oxidation and sonication has rarely been described with respect to practical application. Thus, we present a comparative study on oxidation and sonication processing using MZVI and nZVI at a neutral pH solution with neither the external addition of H_2O_2 nor air sparging in which not only the concentrations of 1,4-D, H_2O_2 , and ionic Fe have been monitored but also the morphology of ZVI before and after reaction has been observed.

2. Materials and methods

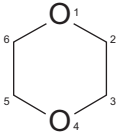
2.1. Chemicals

Hydrogen peroxide (35%), sulfuric acid, NaOH (1M), and sodium chloride were purchased from Junsei. Also, 1,4-D (anhydrous, 99.8%), dichloromethane (>99.5%), anhydrous sodium sulfate, methanol, ethanol, sodium borohydride, ferric chloride hexahydrate (97%, reagent grade), and 2-bromo-1-chloropropane (95%) were obtained from Sigma–Aldrich and used without further purification; 2-bromo-1-chloropropane was used as an internal standard for gas chromatograph (GC) analysis. For measurement of the concentration of H_2O_2 , phthalic acid, ammonium molybdate, and potassium iodide purchased from Sigma–Aldrich were used as received. MZVI was purchased from Acros. Double-distilled water (deionized [DI] water, >18 m Ω) was used for the preparation of all experimental solutions.

2.2. Preparation of MZVI and nZVI

MZVI was immersed in 1% sulfuric acid washed twice with DI water that had been purged with N_2 and freeze-dried for 1 day, while nZVI was prepared by the reduction of Fe^{3+} in an aqueous 0.05M ferric chloride hexahydrate solution with 0.25M sodium borohydride. According to the standard protocol, 200 ml borohydride solution was added to a 200-ml ferric solution under an N_2 atmosphere [25,27–29]. After 20 min, the floating black nZVI was collected by centrifugation and was washed with ethanol to prevent corrosion. Moisture in the nZVI was removed by filtering and drying the sample in a vacuum oven for 1 day. The measured size distributions of disperse MZVI and nZVI in ethanol solution showed 44 ± 5 and $1.35 \pm 0.40 \mu\text{m}$, respectively.

Table 1
Physicochemical properties of 1,4-dioxane

Chemical structure	
Chemical formula	C ₄ H ₈ O ₂
Molecular weight	88.11
Water solubility	4.31 × 10 ⁵ mg/L
Density	1.02 g/mL
Vapor pressure	4 kPa at 20°C
Boiling point	101.1°C at 101.3 kPa

2.3. Experimental procedures and analytical methods

MZVI loading (0, 0.1, 0.2, 0.5, and 1.0 g/L) and nZVI loading (0.05, 0.1, 0.2, and 0.5 g/L) were examined for the kinetics of 1,4-D removal using 250-ml conical flasks with no lids that contained 100 mL of the initial 100 mg/L of 1,4-D in a horizontal shaker (130 rpm) dynamically to contact air easily for ZVI oxidation. For the ZVI sonication process, the prepared flasks following the above protocol were put in an ultrasonic bath sonicator (40 kHz, 185 W) where filled water was displaced periodically to maintain the temperature of flasks. All experiments were carried out at room temperature (±2°C). Both oxidation and sonication were conducted for 6 h. To quench the ·OH radicals from reacting with 1,4-D, 50 µL of 1 M NaOH and 50 µL of methanol were injected into the sample vials, which were withdrawn at specific time intervals during reactions. The samples were immediately filtered through a syringe filter (0.02 µm pore size, 25 mm diameter, Whatman[®], England). Liquid–liquid extraction by dichloromethane was performed with a GC (Hewlett–Packard 6890, USA) equipped with a flame ionization detector (FID) [36]. Prepared samples (2 µL) were directly injected into the GC/FID with an internal standard. The column (HP-5, phenylmethylsiloxane, USA) was held at 40°C for 4 min, increased to 100°C at 10°C/min, held at 100°C for 2 min, increased to 160°C at 20°C/min, and then held at 160°C for 5 min. As a reference experiment, N₂-purged (5 L/min) runs at each optimal reaction rate for ZVI loading were conducted under identical conditions.

The total ionic Fe concentration was measured by inductively coupled plasma-mass spectroscopy (ICP-MS, Perkin–Elmer, USA, <0.01 mg/L of total Fe ions detection limit). The concentration of released Fe²⁺ ions was determined by the capacity of the reaction between Fe²⁺ ions and 1,10-phenanthroline to yield Fe

(1,10-phenanthroline)³⁺, which was detected by spectrophotometry (Optizen 3220UV, Mecasys, Korea) at 510 nm [30,31,37]. Furthermore, the H₂O₂ concentration was determined using a procedure similar to that reported in the literature procedure via the I³⁻ method at 351 nm with UV–vis spectrophotometry [29]: potassium iodide (33 g), sodium hydroxide (1 g), and ammonium molybdate tetrahydrate (0.1 g) were dissolved in DI water to become 500 mL in flasks. Solutions were subsequently mixed with potassium hydrogen phthalate (10 g) in DI water at the same volume. By mixing with the appropriate reaction volume adjusted with DI water, the mixtures were subsequently analyzed. A pH meter (model 710, Thermo Orion, USA) was used to monitor the pH variations during the reaction. All experiments were performed in duplicate, and the results are plotted as average values.

2.4. Characterization of MZVI and nZVI

Morphological characterization of the catalysts was performed by transmission electron microscopy (TEM; JEM-2100F, JEOL Ltd., Tokyo, Japan) and scanning electron microscopy (SEM; S4800, Hitachi, Tokyo, Japan). Powder X-ray diffraction (PXRD) patterns of the catalysts were examined by D/MAX-IIIC (3 kW) with Cu Kα radiation. N₂ sorption/desorption data were obtained using a gas sorption analyzer (NOVA[®] 4200 Ver. 7.10, USA) to assess with the Brunauer, Emmett, and Teller (BET) method.

3. Results and discussion

3.1. Kinetics of 1,4-D degradation under the open-air system (without air purging)

To examine the degradation kinetics of 1,4-D in the ZVI oxidation and sonication processes, it was evaluated with pseudo-first-order and pseudo-second-order kinetic model to determine which model was best fitted by the experimental data. The kinetic data by pseudo-first-order kinetics is based on the following equation:

$$\ln \frac{C_0}{C} = k_1 t$$

where C is the 1,4-D concentration at a given time t (min), C_0 is the initial 1,4-D concentration (mg/L), and k_1 is the observed pseudo-first-order rate constant (min⁻¹) [23], while pseudo-second-order kinetics results in the following kinetic rate expression:

$$\frac{1}{C} - \frac{1}{C_0} = k_2 t$$

where k_2 is the observed pseudo-second-order rate constant (L/mg min) and other parameters are identical as mentioned above [38].

Fig. 1 and Table 2 show results of the pseudo-first-order and pseudo-second-order kinetic plots as functions of ZVI loading for oxidation and sono-Fenton at room temperature, based on Fig. 1. The kinetic constants obtained by linear regression from the two kinetic equations are summarized in Table 2. The correlation coefficients for the pseudo-first order model and the pseudo-second-order model for MZVI and nZVI were similar, indicating that it is difficult to determine which kinetic model was better matched. However, in sono-Fenton system of MZVI and nZVI, it is better fitted with the pseudo-second-order model rather than with the pseudo-first-order model, following a 1,4-D concentration-dependent reaction.

It is important to break the cyclic ether ring of 1,4-D because the by-products of 1,4-D are organic acids such as formic, methoxyacetic, acetic, glycolic, glyoxylic, and oxalic acids which are easily biodegradable [2]. As shown in Fig. 1, the removal of 1,4-D was rapid during the initial stage but slightly reduced in all cases, due to iron corrosion of and the inhibition of Fe^0 [24]. Overall, the reaction rates of oxidation and sonication in the presence of MZVI were higher than those of nZVI at the equivalent loadings of ZVI at neutral pH. The removal efficiency (%) was 60.00 ± 0.35 and $76.65 \pm 0.55\%$ during oxidation and sonication processes, respectively, at an equivalent MZVI loading of 0.5 g/L, thereby resulting in an approximately 16.65% enhancement. In contrast, oxidation in the presence of nZVI exhibited optimal loading at 0.2 g/L with $47.13 \pm 0.24\%$ removal efficiency, while sonication in the presence of 0.1 g/L nZVI exhibited a $60.98 \pm 0.40\%$ removal efficiency, leading to an enhancement of approximately 13.85% from oxidation to sono-Fenton. For the optimal reaction time to meet

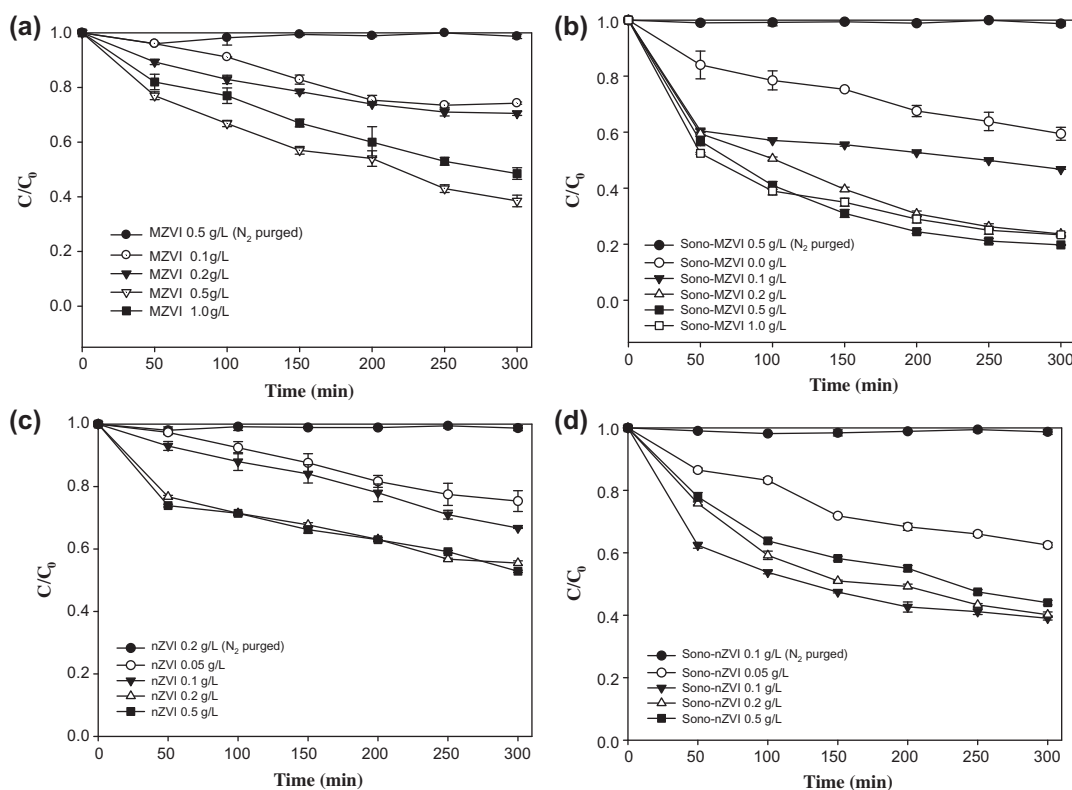


Fig. 1. Time course (C/C_0) of 1,4-D degradation by oxidation (a, c) of MZVI and nZVI and sono-Fenton reaction (b, d) of MZVI and nZVI in an open system, respectively where C and C_0 indicate 1,4-D concentration (mg/L) at a given time t and 0; loadings of MZVI and nZVI were selected to be 0.1/0.2/0.5/1.0 g/L, and 0.05/0.1/0.2/0.5 g/L respectively, initial 1,4-D concentration was 100 mg/L, and all control experiments (i.e. N_2 purged) at optimal ZVI loading were conducted. In (b), sono-MZVI 0.0 g/L indicates sonication treatment without ZVI. Values in bar graphs are mean \pm s.d. of two independent experiments.

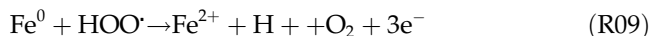
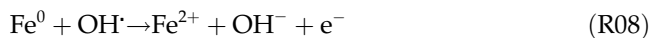
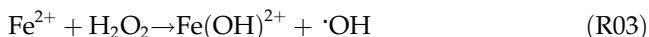
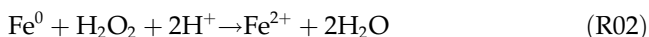
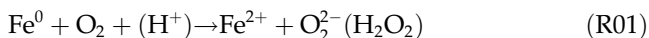
Table 2

The observed kinetic constants of MZVI and nZVI for oxidation and sono-Fenton

	ZVI loading (g/L)	Pseudo-first-order		Pseudo-second-order	
		k_1 (min ⁻¹)	R_1^2	k_2 (L/mg min)	R_2^2
Oxidation (MZVI)	0.1	0.0012	0.941	1.2009	0.935
	0.2	0.0012	0.935	1.2465	0.960
	0.5	0.0030	0.980	4.5320	0.980
	1.0	0.0024	0.990	3.0764	0.992
Sono-Fenton (MZVI)	0	0.0016	0.968	1.8918	0.984
	0.1	0.0020	0.712	2.6812	0.800
	0.2	0.0046	0.955	9.5521	0.993
	0.5	0.0053	0.928	12.4320	0.991
	1.0	0.0044	0.879	9.3891	0.978
Oxidation (nZVI)	0.05	0.0010	0.988	1.0392	0.986
	0.1	0.0013	0.992	1.4528	0.981
	0.2	0.0018	0.910	2.2079	0.951
	0.5	0.0018	0.890	2.2263	0.934
Sono-Fenton (nZVI)	0.05	0.0015	0.953	1.7503	0.971
	0.1	0.0028	0.835	4.2971	0.921
	0.2	0.0029	0.9243	4.268	0.973
	0.5	0.0026	0.949	3.593	0.983

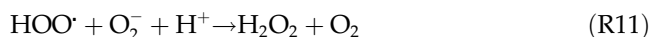
<0.05 mg/L of 1,4-D concentration, reactions were further proceeded to reach that regulation satisfactorily: at 10 and 8 h of MZVI, 15 and 10 h of nZVI for oxidation and sono-Fenton, respectively (data not shown).

As a result, the effect of sonication on 1,4-D degradation was slightly greater in the presence of MZVI than that in the presence of nZVI. As the highest amount of ZVI was loaded in both processes, the 1,4-D removal efficiency was reduced. This finding implies that the removal of 1,4-D in heterogeneous systems occurs mainly in the bulk solution rather than adsorption on the surface of ZVI, i.e. the degradation involves access to 1,4-D in the bulk solution [29]. Taking the 1,4-D degradation mechanism into account [2,4,9–11], the reaction equations related to ZVI oxidation and sonication at (near) neutral pH (<7.4) are as follows:



The attackers degrading 1,4-D were $\cdot\text{OH}$ radicals as well as Fe^{4+} species at neutral pH [5,6], whose $\cdot\text{OH}$ radicals were generated by reacting Fe^{2+} and the H_2O_2 that was spontaneously produced in the presence of Fe^0 and O_2 . Furthermore, because the pH level during the reactions under all conditions was maintained at ~ 6.5 (data not shown), the ZVI catalyst promoted the ferryl ion (Fe^{4+}) to a pH of >5.0 [6,16,28]. Even though Fe^0 recycled Fe^{3+} to Fe^{2+} , the OH^- ions at neutral pH complexed with Fe^{3+} ions, leading to the rapid formation of precipitated $\text{Fe}(\text{OH})_3$ (Eq. (R06)). Sonication

may be used to improve target organics degradation at neutral pH despite the introduction of an additional energy cost. In addition to the above equations, sonication in the presence of ZVI (sono-Fenton) at neutral pH involves more complex equations [29,30]:



The above equations show that more diverse free radicals are produced, and the additional $\cdot\text{OH}$ and HOO^\cdot radicals might be accelerated by H_2O_2 sonolysis (Eqs. (R14)–(R16)). Moreover, the process of sonication not only produces H_2O_2 from H_2O (Eqs. (R11) and (R17)) but also generates $\cdot\text{OH}$ radicals from H_2O (Eq. (R18)).

To further investigate the inhibition effect of the highest ZVI loading, we attempted to remove 1,4-D with ultrasound irradiation alone: sonolysis conducted without ZVI for 1,4-D removal yielded a rate of 0.16×10^{-2} 1/min (Fig. 1(b) and Table 2), which is similar to the results obtained by other authors [24]. The concentration of Fe^{2+} ions released from Fe^0 that reacted with $\cdot\text{OH}$ radicals accelerated with increasing Fe^0 loadings. Therefore, Fe^0 may compete with 1,4-D in the $\cdot\text{OH}$ radical reaction, which is a mechanism that is similar to that suggested for the initiation step of the sono-Fenton process [24,39,40]. However, in this experiment, the competition did not occur significantly, and the acceleration step was not present either.

From 1,4-D degradation data, it can be concluded that the smaller size of ZVI does not play a decisive

role in the enhancement of 1,4-D degradation at neutral pH. Thus, to date, studies of the bulk solution and ZVI characteristics should be examined. Control experiments for all cases were performed during N_2 purging to verify the degradation of 1,4-D (Fig. 1). Slight 1,4-D degradation under all conditions was observed. This degradation can be related to the reduced release of Fe ions into the solution, thereby significantly reducing the production of $\cdot\text{OH}$ radicals and Fe^{4+} species [30]. This finding indicates not only that the ionic Fe concentration is an important factor for oxidation and sonication processes in the presence of ZVI but that Fe corrosion is required for the release of Fe ions into the bulk solution [35]. Interestingly, 1,4-D adsorption onto ZVI surfaces and the direct cleavage of 1,4-D in the ZVI during both oxidation and sonication processes did not occur (Fig. 1). This reason is associated with the limitless water solubility and recalcitrant molecular structure of 1,4-D as described in the Introduction; these results are different from those reported for dye removal by the ZVI/air technique [34].

3.2. Measurement of ionic Fe and H_2O_2 generation

As shown in Fig. 2, the concentration of ionic Fe released during the oxidation process was lower than that released during the sono-Fenton process. Ionic Fe was initially released rapidly under all conditions; the concentration was gradually reduced during the oxidation process but showed different behavior in the sono-Fenton system, possibly meaning that the iron oxide formation of ZVI appeared initially within 1 h [30]. The ionic Fe concentrations for MZVI and nZVI oxidation were maintained at <0.5 and <0.2 mg/L and almost reached a quasi-equilibrium state at ~ 0.3 and 0.01 mg/L, respectively. At increased MZVI loading, the concentration of released ionic Fe showed an increasing trend during both the oxidation and sono-Fenton reaction. However, low loading of nZVI during the oxidation process produced a higher concentration of released ionic Fe, and, during the sono-Fenton reaction, significantly increased the concentration of ionic Fe released (the highest concentration among all conditions: ~ 4 mg/L), which quickly decreased to an equilibrium state, <1 mg/L at 0.5 g/L loading of nZVI [31]; this finding resulted in the oxidation or, presumably, the precipitation of ionic Fe on the surface of ZVI at neutral pH [31]. Interestingly, a MZVI loading of 1.0 g/L in the sono-Fenton process reduced the solution pH from 7.0 to 5.5 (data not shown). Decrease of pH was associated with production of acidic by-products and reduction of OH ions

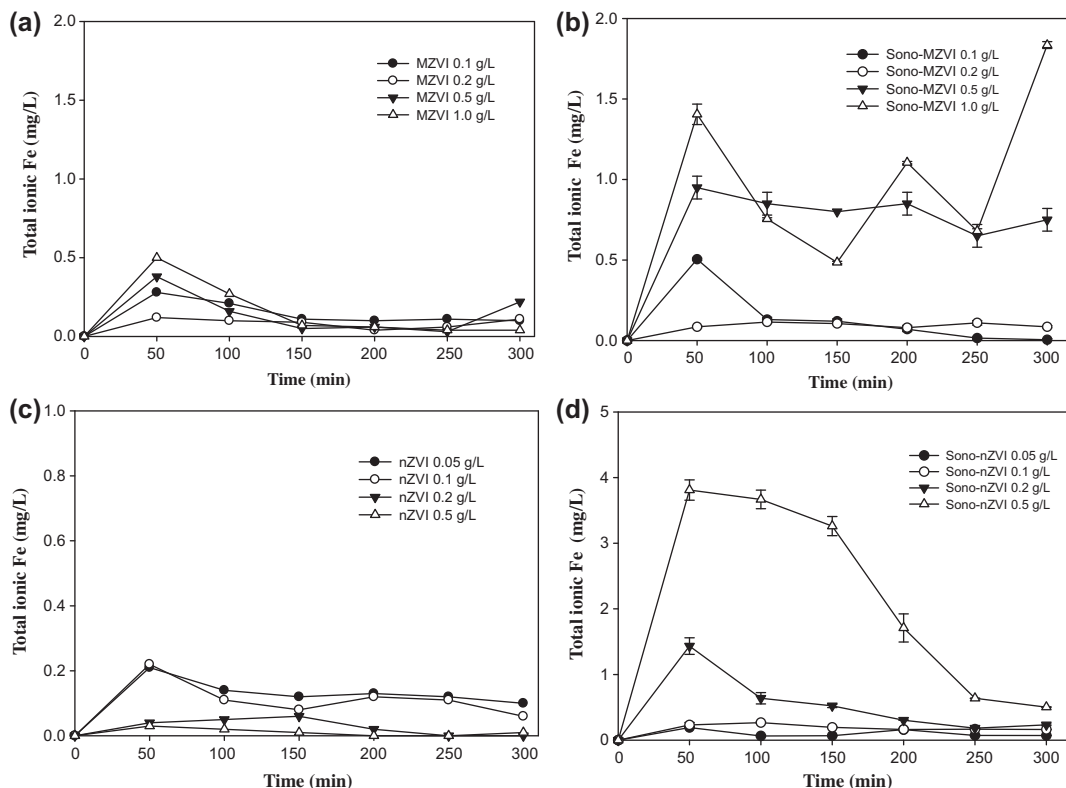


Fig. 2. Released Fe ion concentration (mg/L) by oxidation (a, c) and sono-Fenton reaction (b, d) of MZVI and nZVI, respectively.

by $\text{Fe}(\text{OH})_3$ deposition onto the MZVI surface [2]. A further increase in MZVI loading would not be expected to increase the 1,4-D removal efficiency.

These processes affected the ZVI surface morphology, which will be discussed in Section 3.3. Taking the 1,4-D degradation efficiency into consideration, approximately 1 mg/L of released ionic Fe would be the best concentration (Fig. 2(b)), and steadily maintaining the ionic Fe concentration during reaction is important. Furthermore, in the control experiment (N_2 purged), the concentration of released ionic Fe was below the detection limit of 0.01 mg/L. This finding indicates that the inhibition of ZVI corrosion in the absence of oxygen may block the dissolution of Fe^{2+} ions into solution [30]. In addition, the concentration of Fe^{2+} ions was similar to the concentration of total Fe ions, which implies that most of the ionic Fe present as Fe^{2+} ion was initially released and subsequently oxidized to Fe^{3+} and transformed into $\text{Fe}(\text{OH})_3$ precipitate as the reaction proceeded. This finding is in line with the fact that the concentration of released ionic Fe measured by ICP-MS was similar to the Fe^{2+} concentration measured by UV-vis spectrophotometry.

However, although the ionic Fe concentration that was released is shown to have been the highest in

Fig. 2(d), the H_2O_2 concentration should also be considered. Fig. 3 shows that the concentration of H_2O_2 fluctuated during all of the reactions. The burst of H_2O_2 generation at the start of the reaction enhanced the 1,4-D degradation efficiency, but the efficiency decreased progressively as H_2O_2 was eliminated through reaction with $\cdot\text{OH}$ radicals (R14). For the oxidation process, the levels of H_2O_2 generation in both MZVI and nZVI were similar, although MZVI produced less compared to nZVI. In contrast, the nZVI sono-Fenton process is more sensitive to variations in the H_2O_2 concentration than in the MZVI process. Within 3 h of reaction, the H_2O_2 concentration in 0.5 g/L MZVI and 0.1 g/L nZVI was approximately 50 and >60 mM, respectively, but as time elapsed, the H_2O_2 concentration was significantly reduced to ~ 10 and ~ 20 mM, respectively. The reason for decrease in 1,4-D degradation efficiency at the highest loading of 0.5 g/L nZVI in sono-Fenton process might be related to decrease in H_2O_2 generation, which is due to consumption of Fe^0 sites competitively [4], indicating that size of ZVI is not decisive during 1,4-D degradation efficiency. Therefore, it is plausible that the low removal efficiency of 1,4-D in the nZVI sono-Fenton process compared to that of the MZVI sono-Fenton

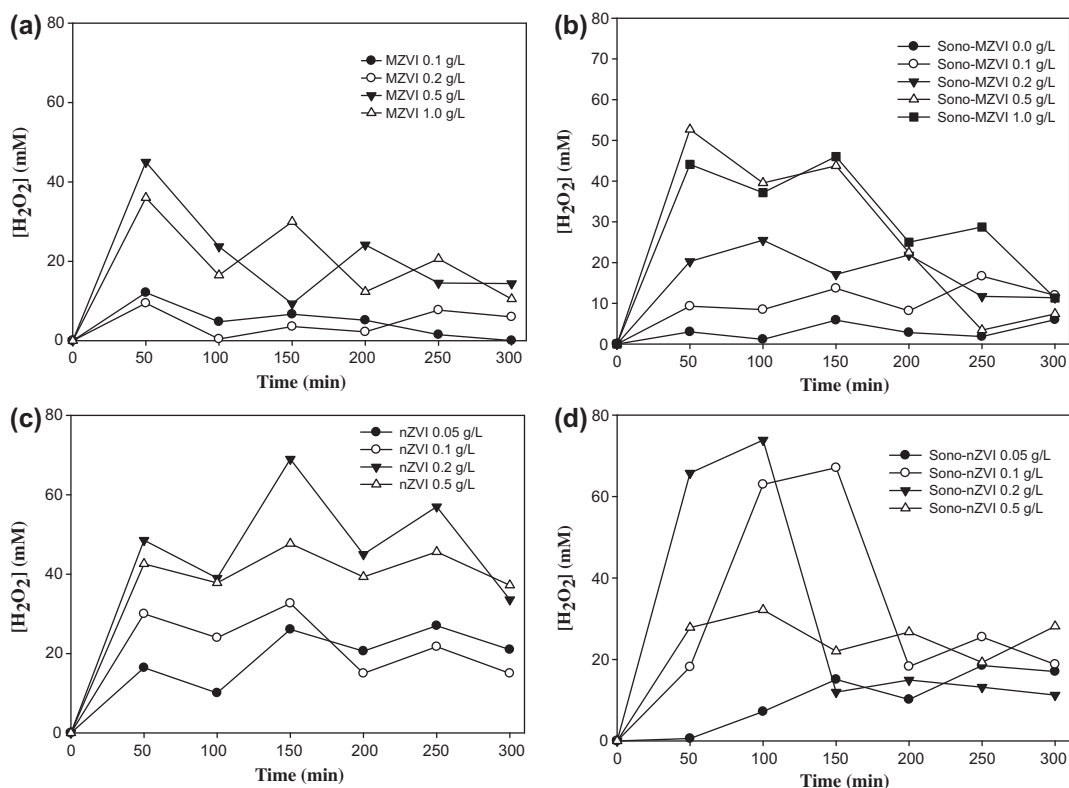


Fig. 3. Variations in H_2O_2 concentration (mM) by oxidation (a, c) and sono-Fenton reaction (b, d) of MZVI and nZVI, respectively.

process was significantly affected by the concentration of released ionic Fe.

In conclusion, even though the reactions are heterogeneous (surface-mediated) in the ZVI system, the degradation reaction was predominant in the bulk solution, indicating the released ionic Fe and H_2O_2 coexisted, which have a crucial combination in producing oxidant attackers, $\cdot\text{OH}$ free radicals and Fe^{4+} species; for the removal of 1,4-D, the optimal ionic Fe and H_2O_2 concentrations are approximately 1 mg/L and 10–20 mM in MZVI sono-Fenton system, respectively. To enhance the degradation efficiency, the most important factor for the two parameters is sustainability during reactions. Thus, ZVI was continuously oxidized and released ionic Fe as well as new Fe^0 surfaces to react with O_2 and thus produce H_2O_2 until reaction termination [35]. Taking the optimization of two parameters into consideration in this system, therefore, it is useful to plan as a suitable model.

3.3. Morphological observation of ZVI

The surface morphology of both fresh MZVI and as-prepared nZVI before and after reaction is shown in Figs. 4 and 5. The plate-like stacked structures

present in the micrometer-sized crystals of MZVI were examined; the area indicated by the dotted circle in Fig. 2(c) was observed in typical MZVI surfaces [23] (Fig. 4(a)–(c)). On the other hand, the diameters of nanowire-like nZVI ranged between 20 and 100 nm (Fig. 4(d) and (e)). The high-magnification TEM images show a shell with a thickness of ~ 5 nm (the amorphous region), and the cubic $\text{Fe}(0)$ structure was confirmed by selected-area electron diffraction (SAED), which was within the range of the previously reported values (1–25 nm) (Fig. 4(f) and inset) [27,28]. It is suggested that the nanowires formed via the self-assembly of nuclei through borohydride reduction [27–29,32].

After oxidation, MZVI and nZVI showed slightly altered morphologies. MZVI was reduced to plates, though a stacking structure can still be discerned (Fig. 5(a) and (b)), while nZVI particles were transformed into disconnected chains and a few short-chained particles (Fig. 5(e) and (f)). Sono-Fenton treatment had an effect on the morphologies of MZVI and nZVI. Fig. 5(c) and (d) show that the surface morphology of MZVI remained unchanged after sono-Fenton treatment, except for a loosely stacked, plate-like structure and a partially transformed, needle-like

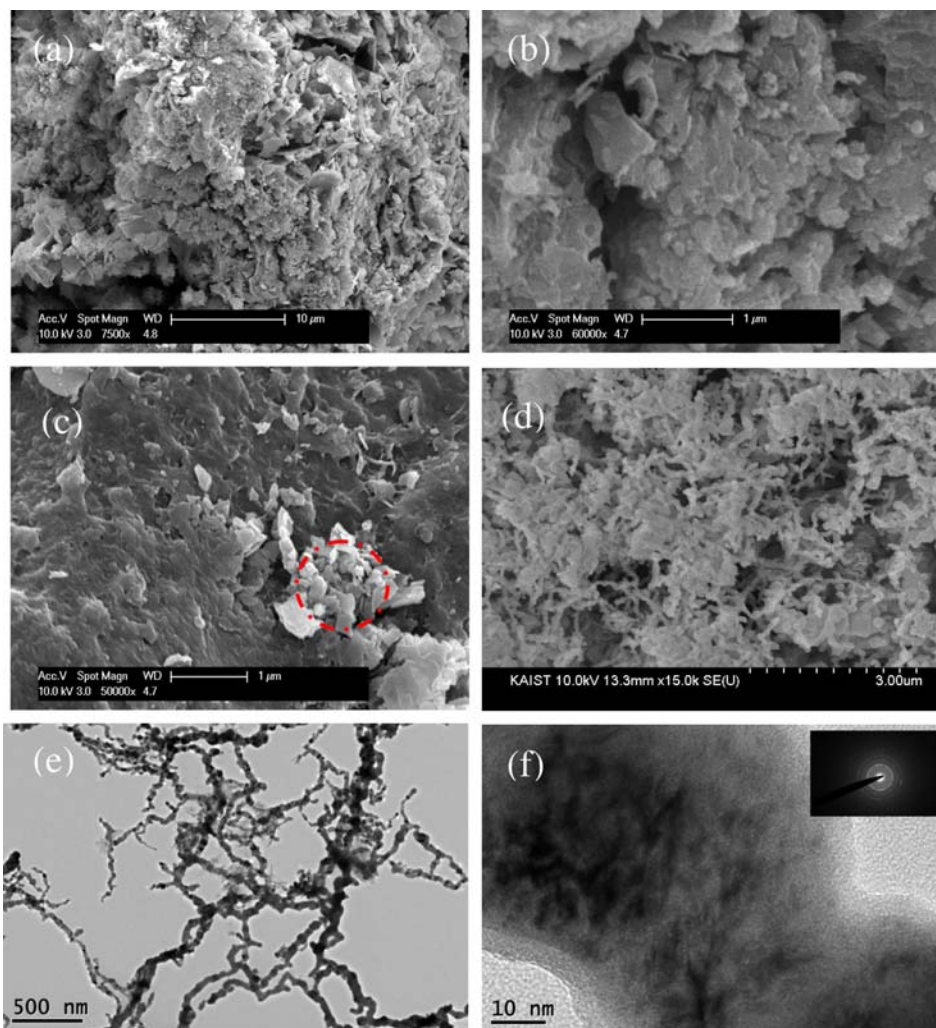


Fig. 4. SEM images at low magnification (a) and high magnification (b, c) of fresh MZVI. SEM image (d) and TEM images (e) at low magnification of as-prepared nZVI. TEM image (f) at high magnification with as-prepared nZVI. The inset of (f) is the selected area electron diffraction pattern (SAED) of as-prepared nZVI. Note: dotted circle in (c) indicates dense MZVI particles.

structure in the micrometer-sized crystal plates (Fig. 5 (c)), which resulted in an increased surface area, which retains different surface pitting effects caused by shock waves on the surface of iron [18,22]. Although the oxidative catalyst activity of MZVI could be slightly reduced, the interesting morphology shown in Fig. 5(d) promoted the retention of catalytic activity during longer reactions and ultimately functioned to regenerate the catalyst, which is supported by PXRD patterns (see Section 3.4). It should be noted that the needle-like structure of MZVI was present within only a small subset of samples, and MZVI structures mostly retained their original morphology after the sono-Fenton reaction. In contrast, after the sono-Fenton process, the nanowire-like structures of nZVI broke into spherical particles with diameters

ranging from 18 to 80 nm (Fig. 5(g) and (h)). Some particles were greater than 100 nm in size, due to their magnetic properties. These results are consistent with increased BET surface areas of the catalysts after reactions. After the oxidation and sono-Fenton reactions, the BET surface area values of MZVI and nZVI increased from 0.68 to 1.77 to 2.77 m²/g and from 25.01 to 34.38 to 63.33 m²/g, respectively. Ultrasonic treatment of the nanoparticles not only produced uniform spherical structures but also cleaned the ZVI surface [18,23]. The sono-Fenton process facilitated the breakdown of ZVI into loosely disconnected or randomly aggregated structures with much rougher surfaces, probably due to the formation of iron oxide on the surfaces. Thus, we can assume that iron oxide is formed from free Fe ions on the surface of ZVI. This

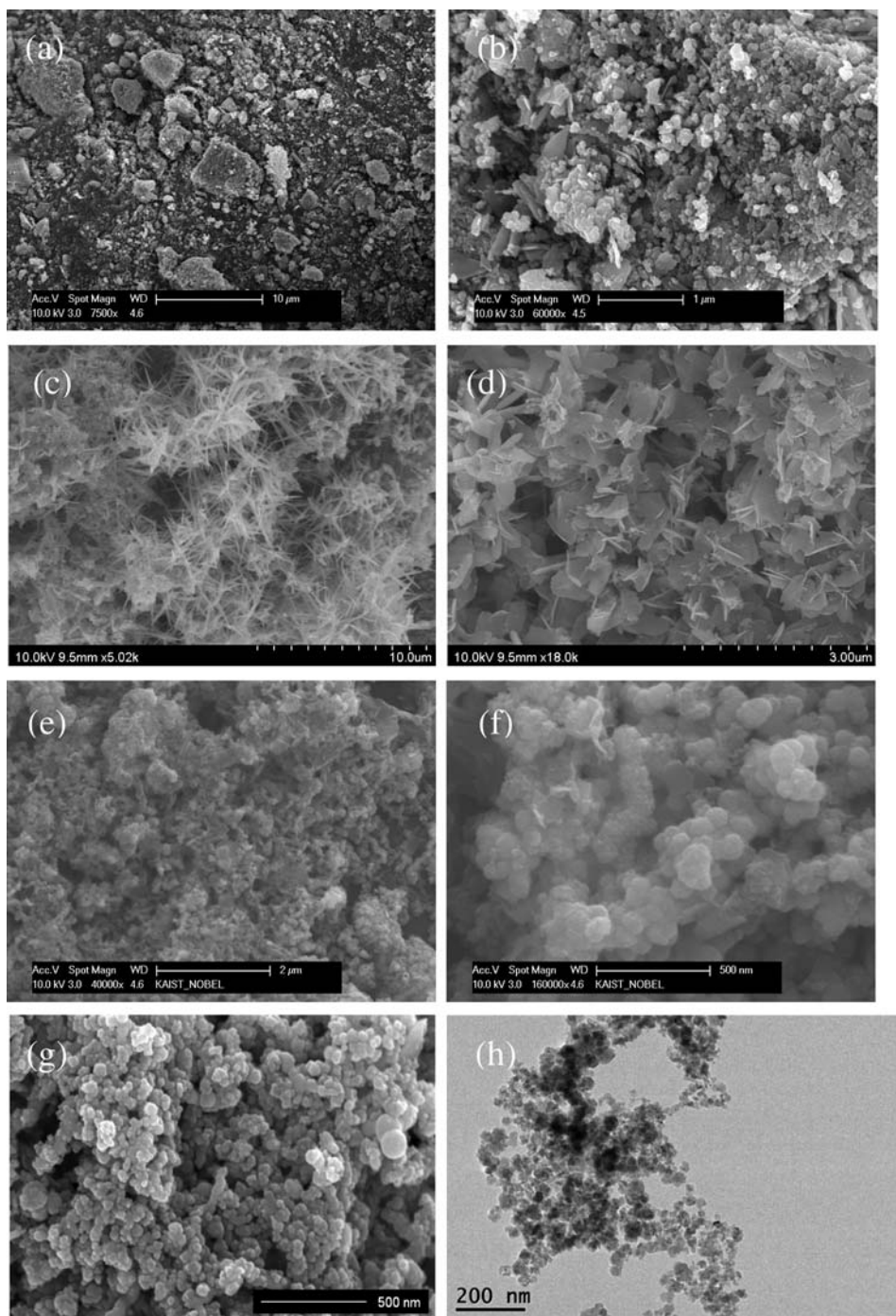


Fig. 5. SEM images at low magnification (a, c) and high magnification (b, d) of MZVI after oxidation and sono-Fenton reaction. SEM images at low magnification (e, f) of nZVI after oxidation, SEM image (g) and TEM image (h) of nZVI after sono-Fenton reaction.

postulation is supported by the result of Ai et al. [31], who concluded that free Fe ions nucleate and grow into iron oxide ($\gamma\text{-Fe}_2\text{O}_3/\text{Fe}_3\text{O}_4$) layers on the surface of ZVI.

3.4. PXRD studies

The PXRD patterns for both fresh MZVI and as-prepared nZVI included sharp intensity peaks at $\sim 2\theta = 45^\circ$ and 65° , which corresponded to the

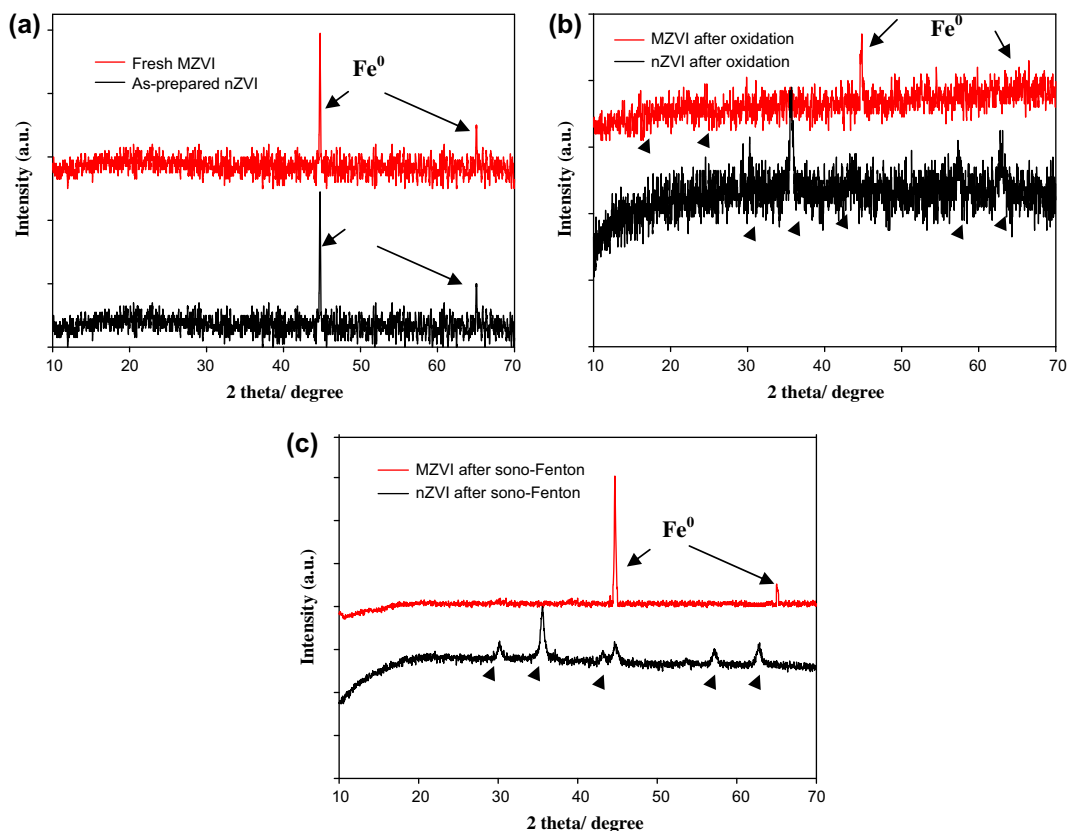


Fig. 6. PXRD patterns of (a) fresh MZVI and as-prepared nZVI, (b) MZVI and nZVI after oxidation, and (c) MZVI and nZVI after sono-Fenton reaction. Note: filled triangles denote Fe_3O_4 in (b) and $\gamma-Fe_2O_3/Fe_3O_4$ in (c), respectively.

body-centered cubic Fe lattice (Fig. 6(a)), which was analogous to the SAED of inset of Fig. 4(f). Although bulk nZVI powder featured iron oxide on its particle surfaces, no XRD patterns could be discerned because the iron oxide was amorphous and too small (below 5 nm), to be detected [27,28]. After the oxidation process, bulk MZVI powder was oxidized, producing an Fe^0 peak intensity, while nZVI was almost converted to iron oxide (Fe_3O_4), resulting in a loss in oxidation catalytic activity (Fig. 6(b)).

However, Fig. 6(c) shows that the MZVI in large part retained the standard Fe^0 peak, even after 5 h of sono-Fenton processing. In addition, the sharp standard Fe^0 peak in nZVI almost disappeared and was replaced by the distinct $\gamma-Fe_2O_3/Fe_3O_4$ pattern as the transformation of ZVI proceeded. Although we cannot rule out the coexistence of minor Fe^0 in nZVI after oxidation and sono-Fenton processes, nZVI did not improve the kinetic profile of 1,4-D relative to its treatment with MZVI. The conserved Fe^0 in MZVI after the sono-Fenton reaction implies that the potential for recycling and reusing ZVI catalysts is unlimited [41].

3.5. Environmental implications

ZVI oxidation and sono-Fenton processing for the degradation of pollutant organics is effective without the need to externally supply H_2O_2 at neutral pH because it can reduce the complex steps typically required to discharge pollutants after treatment, resulting in cost reduction from a practical applications perspective. Unfortunately the increased surface area of nZVI did not enhance 1,4-D degradation at neutral pH significantly. This low degradation of 1,4-D was due to fast oxidation of nZVI itself. To be used effectively as an oxidation catalyst, ZVI was continuously oxidized and exposed to an Fe^0 surface to produce H_2O_2 . Therefore, MZVI resulted in higher 1,4-D degradation efficiency during both the oxidation and sono-Fenton process. In addition, the concentration of released ionic Fe was regulated (<3 mg/L), and it was determined that the H_2O_2 concentration should be low to prevent any toxic effect. As a result, in the case of nZVI, previous studies regarding the use of ligands, such as oxalate, nitrilotriacetic acid (NTA), and ethylenediaminetetracetic acid (EDTA), were referenced to limit iron precipitation [16,17,42].

4. Conclusions

In summary, the optimal loading concentrations of ZVI for 1,4-D degradation in oxidation and sono-Fenton systems were same 0.5 g/L for an MZVI system, while 0.2 and 0.1 g/L for an nZVI system at a neutral pH.

In the MZVI sono-Fenton reaction, the optimal ionic Fe and H₂O₂ concentrations were ~1 mg/L and 10–20 mM, respectively, where the sustainability of both concentrations during reaction was important for 1,4-D degradation efficiency, thereby resulting in the modulation of the ·OH radical and Fe⁴⁺ species concentration at neutral pH. To use ZVI efficiently as an oxidation catalyst, ZVI was continuously oxidized, and subsequently released ionic Fe was exposed to Fe⁰ surfaces to generate H₂O₂. Therefore, smaller ZVI particles were not suitable (herein MZVI, 0.68 m²/g; nZVI, 25.01 m²/g); this discrepancy suggests that the optimal ZVI particle size should be determined by further study. Thus, it is anticipated that the present results can provide information regarding the size effect of ZVI-based oxidation technology at a neutral pH for recalcitrant organic compounds in water/wastewater treatment. Studies are currently underway regarding the mixing of different-sized ZVI particles in an air-purging system or magnetic field [43] to enhance the degrading efficiency of non-biodegradable organic compounds.

Acknowledgments

This work was supported by the Advanced Biomass R&D Center (ABC) of Korea Grant funded by the Ministry of Education, Science and Technology (ABC-2011-K000908). We would also like to thank Dr. Jung Ho Yoo in Measurement and Analysis Team of the National NanoFab Center (NNFC) for fruitful discussions about SEM and TEM imaging.

References

- [1] J.Y. Choi, Y.-J. Lee, J. Shin, J.-W. Yang, Anodic oxidation of 1,4-dioxane on boron-doped diamond electrodes for wastewater treatment, *J. Hazard. Mater.* 179 (2010) 762–768.
- [2] C.G. Kim, H.J. Seo, B.R. Lee, Decomposition of 1,4-dioxane by advanced oxidation and biochemical process, *J. Environ. Sci. Health A* 41 (2006) 599–611.
- [3] M.J. Zenker, R.C. Borden, M.A. Barlaz, Occurrence and treatment of 1,4-dioxane in aqueous environments, *Environ. Eng. Sci.* 20 (2003) 423–432.
- [4] H.S. Son, J.K. Im, K.D. Zoh, A Fenton-like degradation mechanism for 1,4-dioxane using zero-valent iron (Fe⁰) and UV light, *Water Res.* 43 (2009) 1457–1463.
- [5] S.H. Joo, A.J. Feitz, T.D. Waite, Oxidative degradation of the carbothioate herbicide, molinate, using nanoscale zero-valent iron, *Environ. Sci. Technol.* 38 (2004) 2242–2247.
- [6] A.J. Feitz, S.H. Joo, J. Guan, Q. Sun, D.L. Sedlak, T.D. Waite, Oxidative transformation of contaminants using colloidal zero-valent iron, *Colloid Surf. A—Physicochem. Eng. Asp.* 265 (2005) 88–94.
- [7] S.E. Mylon, Q. Sun, T.D. Waite, Process optimization in use of zero valent iron nanoparticles for oxidative transformations, *Chemosphere* 81 (2010) 127–131.
- [8] C.R. Keenan, D.L. Sedlak, Factors affecting the yield of oxidants from the reaction of nanoparticulate zero-valent iron and oxygen, *Environ. Sci. Technol.* 42 (2008) 1262–1267.
- [9] C.D. Adams, P.A. Scanlan, N.D. Secrist, Oxidation and biodegradability enhancement of 1,4-dioxane using hydrogen peroxide and ozone, *Environ. Sci. Technol.* 28 (1994) 1812–1818.
- [10] R.R. Hill, G.E. Jeffs, D.R. Roberts, Photocatalytic degradation of 1,4-dioxane in aqueous solution, *J. Photochem. Photobiol. A* 108 (1997) 55–58.
- [11] V. Maurino, P. Calza, C. Minero, E. Pelizzetti, M. Vincenti, Light-assisted 1,4-dioxane degradation, *Chemosphere* 35 (1997) 2675–2688.
- [12] M.I. Stefan, J.R. Bolton, Mechanism of degradation of 1,4-dioxane in dilute aqueous solution using the UV/hydrogen peroxide process, *Environ. Sci. Technol.* 32 (1998) 1588–1595.
- [13] M. Pera-Titus, V. García-Molina, M.A. Baños, J. Giménez, S. Esplugas, Degradation of chlorophenols by means of advanced oxidation processes: A general review, *Appl. Catal. B—Environ.* 47 (2004) 219–256.
- [14] T. Zhou, Y. Li, J. Ji, F.S. Wong, X. Lu, Oxidation of 4-chlorophenol in a heterogeneous zero valent iron/H₂O₂ Fenton-like system, *Sep. Purif. Technol.* 62 (2008) 551–558.
- [15] C. Lee, D.L. Sedlak, Enhanced formation of oxidants from bimetallic nickel-iron nanoparticles in the presence of oxygen, *Environ. Sci. Technol.* 42 (2008) 8528–8533.
- [16] C.R. Keenan, D.L. Sedlak, Ligand-enhanced reactive oxidant generation by nanoparticulate zero-valent iron and oxygen, *Environ. Sci. Technol.* 42 (2008) 6936–6941.
- [17] C. Lee, C.R. Keenan, D.L. Sedlak, Polyoxometalate-enhanced oxidation of organic compounds by nanoparticulate zero-valent iron and ferrous ion in the presence of oxygen, *Environ. Sci. Technol.* 42 (2008) 4921–4926.
- [18] H.M. Hung, M.R. Hoffmann, Kinetics and mechanism of the enhanced reductive degradation of CCl₄ by elemental iron in the presence of ultrasound, *Environ. Sci. Technol.* 32 (1998) 3011–3016.
- [19] M.A. Beckett, I. Hua, Enhanced sonochemical decomposition of 1,4-dioxane by ferrous iron, *Water Res.* 37 (2003) 2372–2376.
- [20] M.A. Beckett, I. Hua, Elucidation of the 1,4-dioxane decomposition pathway at discrete ultrasonic frequencies, *Environ. Sci. Technol.* 34 (2000) 3944–3953.
- [21] S.N. Nam, S.K. Han, J.W. Kang, H. Choi, Kinetics and mechanisms of the sonolytic destruction of non-volatile organic compounds: investigation of the sonochemical reaction zone using several OH[·] monitoring techniques, *Ultrason. Sonochem.* 10 (2003) 139–147.
- [22] H. Zhang, L. Duan, Y. Zhang, The use of ultrasound to enhance the decolorization of the C.I. Acid Orange 7 by zero-valent iron, *Dyes Pig.* 65 (2005) 39–43.
- [23] Y. Dai, F. Li, F. Ge, F. Zhu, L. Wu, X. Yang, Mechanism of the enhanced degradation of pentachlorophenol by ultrasound in the presence of elemental iron, *J. Hazard. Mater.* B137 (2006) 1424–1429.
- [24] H.S. Son, S.B. Choi, E. Khan, K.D. Zoh, Removal of 1,4-dioxane from water using sonication: Effect of adding oxidants on the degradation kinetics, *Water Res.* 40 (2006) 692–698.
- [25] W.X. Zhang, Nanoscale iron particles for environmental remediation: A review, *J. Nanopart. Res.* 5 (2003) 323–332.
- [26] A.M. Giasuddin, S.R. Kanel, H.C. Choi, Adsorption of humic acid onto nanoscale zerovalent iron and its effect on arsenic removal, *Environ. Sci. Technol.* 41 (2007) 2022–2027.

- [27] Y.-C. Lee, C.-W. Kim, J.-Y. Lee, H.-J. Shin, J.-W. Yang, Characterization of nanoscale zero valent iron modified by non-ionic surfactant for trichloroethylene removal in the presence of humic acid: A research note, *Desalin. Water Treat.* 10 (2009) 33–38.
- [28] J.E. Martin, A.A. Herzing, W. Yan, X. Li, B.E. Koel, C.J. Kiely, W. Zhang, Determination of the oxide layer thickness in core-shell zerovalent iron nanoparticles, *Langmuir* 24 (2008) 4329–4334.
- [29] Z.H. Ai, L.R. Lu, J.P. Li, L.Z. Zhang, J.R. Qiu, M.H. Wu, Fe@Fe₂O₃ core-shell nanowires as iron reagent. 1. Efficient degradation of Rhodamine B by a novel sono-Fenton process, *J. Phys. Chem. C* 111 (2007) 4087–4093.
- [30] T. Luo, Z. Ai, L. Zhang, Fe@Fe₂O₃ core-shell nanowires as iron reagent. 4. Sono-Fenton degradation of pentachlorophenol and the mechanism analysis, *J. Phys. Chem. C* 112 (2008) 8675–8681.
- [31] Z. Ai, L. Lu, J. Li, L. Zhang, J. Qiu, M. Wu, Fe@Fe₂O₃ core-shell nanowires as iron reagent. 2. An efficient and reusable sono-Fenton system working at neutral pH, *J. Phys. Chem. C* 111 (2007) 7430–7436.
- [32] E.-J. Kim, J.-H. Kim, A.-M. Azad, Y.-S. Chang, Facile synthesis and characterization of Fe/FeS nanoparticles for environmental applications, *ACS Appl. Mater. Interf.* 3 (2011) 1457–1462.
- [33] I. Ioan, S. Wilson, E. Lundanes, A. Neculai, Comparison of Fenton and sono-Fenton bisphenol A degradation, *J. Hazard. Mater.* 142 (2007) 559–563.
- [34] S.-H. Chang, S.-H. Chuang, H.-C. Li, H.-H. Liang, L.-C. Huang, Comparative study on the degradation of I.C. Remazol Brilliant Blue R and I.C. Acid Black 1 by Fenton oxidation and Fe⁰/air process and toxicity evaluation, *J. Hazard. Mater.* 166 (2009) 1279–1288.
- [35] T. Zhou, X. Lu, J. Wang, F.-S. Wong, Y. Li, Rapid decolorization and mineralization of simulated textile wastewater in a heterogeneous Fenton like system with/without external energy, *J. Hazard. Mater.* 165 (2009) 193–199.
- [36] Y.M. Park, H. Pyo, S.J. Park, S.K. Park, Development of the analytical method for 1,4-dioxane in water by liquid–liquid extraction, *Anal. Chim. Acta.* 548 (2005) 109–115.
- [37] H. Park, Y.-C. Lee, B.G. Choi, Y.S. Choi, J.-W. Yang, W.H. Hong, Energy transfer in ionic-liquid-functionalized inorganic nanorods for highly efficient photocatalytic applications, *Small* 6 (2010) 290–295.
- [38] P. Wanaratna, C. Christodoulatos, M. Sidhoum, Kinetics of RDX degradation by zero-valent iron (ZVI), *J. Hazard. Mater.* 136 (2006) 68–74.
- [39] W.A. Arnold, A.L. Roberts, Pathways and kinetics of chlorinated ethylene and chlorinated acetylene reaction with Fe(0) particles, *Environ. Sci. Technol.* 34 (2000) 1794–1805.
- [40] J. Kiwi, A. Lopez, V. Nadtochenko, Mechanism and kinetics of the OH radical intervention during Fenton oxidation in the presence of a significant amount of radical scavenger (Cl⁻), *Environ. Sci. Technol.* 34 (2000) 2162–2168.
- [41] Y. Segura, F. Martínez, J.A. Melero, R. Molina, R. Chand, D. H. Bremner, Enhancement of the advanced Fenton process (Fe⁰/H₂O₂) by ultrasound for the mineralization of phenol, *Appl. Catal. B—Environ.* 113–114 (2012) 100–106.
- [42] Y.H. Lee, B.I. Escher, U.V. Gunten, Efficient removal of estrogenic activity during oxidative treatment of waters containing steroid estrogens, *Environ. Sci. Technol.* 42 (2008) 6333–6339.
- [43] D.-H. Kim, J. Kim, W. Choi, Effect of magnetic field on the zero valent iron induced oxidation reaction, *J. Hazard. Mater.* 192 (2011) 928–931.